ELSEVIER

Magnetic Resonance Imaging 20 (2002) 721–731

MAGNETIC RESONANCE IMAGING

Precise estimate of fundamental *in-vivo* MT parameters in human brain in clinically feasible times

A. Ramani*, C. Dalton, D.H. Miller, P.S. Tofts, G.J. Barker

NMR Research Unit, Dept. Clinical Neurology, Institute of Neurology, Queen's Square, University College London, London, WC1N 3BG, England

Received 16 August 2002; accepted 9 September 2002

Abstract

A methodology is presented for extracting precise quantitative MT parameters using a magnetisation-prepared spoiled gradient echo sequence. This method, based on a new mathematical model, provides relaxation parameters for human brain *in-vitro* and *in-vivo*. The *in-vivo* parameters have been obtained from three different regions of normal white matter: occipital white matter, frontal white matter and centrum semiovale; two regions of normal grey matter: cerebral cortex and cerebellum, and from five regions with MS lesions. All this has been achieved using MT images collected within a timeframe that is clinically feasible. We hope that this new technique will shed light on the properties and dynamics of water compartments within the brain. © 2002 Elsevier Science Inc. All rights reserved.

Keywords: Magnetisation transfer; White matter; Multiple sclerosis; Cross-relaxation; Magnetic resonance imaging

1. Introduction

Magnetisation Transfer (MT) imaging has shown great potential for the investigation of white matter diseases, particularly Multiple Sclerosis (MS) [1,2,3]. However, although current commonly used MT imaging techniques can be easily implemented on clinical scanners, the Magnetisation Transfer Ratio (MTR) values usually calculated from these simple, two-point, measurements are "semi-quantitative" in nature. They are sensitive not only to the pathology of interest (e.g. demyelination), but are also affected by other biological changes, such as oedema and inflammation. Moreover, they are difficult to reproduce across sites [4] and tend to reflect a complex combination of sequence details and relaxation parameters [5,6]. Therefore, a more rigorous quantitative approach is needed to extract fundamental MT parameters that might be more specific in characterising the biological changes that take place during pathology, particularly during demyelination, and shed light on tissue structure and organisation. The challenges in implementing such quantitative measurements are twofold: firstly, to devise a model which is simple enough to be useful but still able to encapsulate both the complex biological behaviour and pulse sequence characteristics; secondly, to determine acquisition parameters which allow sufficient data to be collected to fit to the model while remaining in clinical acceptable scanning times.

Several groups of researchers have carried out quantitative studies on the MT phenomenon in an attempt to extract fundamental MT parameters; yet there are few reports published on *in vivo* human brain. Using a binary spin bath model, Chai et al. [7] have attempted to quantify all the parameters by measuring the transient development of the longitudinal magnetisation of the mobile pool using a train of binomial pulses of varying duration and duty cycle. The acquisition time using this method is extremely long (~4 minutes per data point), thus rendering it impractical for patient study. Gochberg et al. [8], using a series of on-resonance inversion pulses in which each pulse selectively inverts the magnetisation of the free pool, and Lee et al. [9], using an off-resonance technique, have both measured the fractional size of the bound pool. The measurement of a only single relaxation parameter, however, has the obvious disadvantage of incomplete description of the MT process. Recently, Sled et al. [10] have used a spoiled gradient-echo sequence that yields all of the relaxation parameters. However, this model is rather complicated since the free pool is described by a modified version of the Bloch equations, while the bound pool makes use of the concept of "inverse spin

Previously presented in an early form at ISMRM, Glasgow 2000 (p 259).

* Corresponding author. Tel.: +44-0-20-7837-3611, ext. 4304; fax: +44-0-20-7278-5616.

E-mail address: a.ramani@nmr.ion.ucl.ac.uk (A. Ramani).

PII: S0730-725X(02)00598-2

temperature" using the Redfield-Provotorov theory [11]. Other problems with this method are long acquisition times, the computation of the saturation fraction using a numerical solution of the Bloch equations and only single-slice imaging capability. A recent article by Vasily [12] describes a technique involving off-resonance saturation pulses to extract *in vivo* relaxation parameters. Although this method offers multi-slice capability, the disadvantages with this method is that the direct saturation effect on the longitudinal magnetisation of the free pool (the so-called "RF bleedover" effect) is assumed to be negligible. Imperfect shimming, non-ideal RF pulse profiles, and the naturally long 'tails' of the free water line mean that this assumption is unlikely to be met *in vivo*. Moreover, the data has been normalised to the fully relaxed magnetisation associated with the free pool (i.e., in MTR format) before being fitted to the model.

In this study, we have implemented modifications to the well-established Henkelman model in order to create a simple model that can accurately reflect the behaviour of the magnetisation during a pulsed MT-weighted imaging sequence. We have implemented the necessary data acquisition for this model in both *in-vitro* and *in-vivo* studies of human brain. Using the model, we have been able to extract quantitative MT parameters that provide information on the fractional size of the bound pool and the relaxation times of the free as well as bound pools.

2. Theory

2.1. Quantitative approach

MT imaging is a technique based on specific interactions between macromolecular protons and water protons. Most of the mathematical models describing MT consist of two pools, the free pool representing the mobile pool of protons and the semi-solid pool representing the macromolecular pool of protons. A quantitative investigation involves the selective saturation of the longitudinal magnetisation associated with the semi-solid pool of protons, using RF irradiation, and the observation of the effect on the free pool of protons [13,14].

Henkelman et al. [13] were amongst the earliest researchers to derive an expression originating from the Bloch formalism describing the steady-state longitudinal magnetisation of the free pool:

$$M_Z^A = \frac{R_B\left[\frac{RM_0^B}{R_A}\right] + R_{\mathrm{RFB}} + R_B + R}{\left[\frac{RM_0^B}{R_A}\right](R_B + R_{\mathrm{RFB}}) + \left(1 + \left[\frac{\omega_1}{2\pi\Delta f}\right]^2\left[\frac{1}{R_A T_2^A}\right]\right)(R_{\mathrm{RFB}} + R_B + R)} \quad (1)$$

where R is the magnetisation transfer rate between the free and semi-solid pools, R_A and R_B are the longitudinal relaxation rates of the free and semi-solid pools respectively, M_0^A and M_0^B are the fully relaxed values of magnetisations associated with the tool pools, T_2^A and T_2^B are the transverse relaxation times of the semi-solid pool, and R_{RFB} is the rate of loss of longitudinal magnetisation by the semi-solid pool due to off-resonance irradiation of amplitude ω_1 and offset frequency Δf. This rate of loss of magnetisation by direct saturation of the semi-solid pool is related to the absorption lineshape of the spins $g(2\pi\Delta f)$ in the semi-solid pool and is given by:

$$R_{\mathrm{RFB}} = \omega_1^2 g(2\pi\Delta f T_2^B) \quad (2)$$

For a detailed derivation of Eq. (1) and a discussion of the binary spin bath model, the reader is directed to references [13,14].

2.2. Calculation of continuous wave power equivalent (B_{1CWPE})

In order to reformulate the well-established in-vitro binary spin-bath model [15], one needs to take into account the pulsed nature of the RF fields available on clinical scanners. Our aim was to create a mathematical model describing acquisitions that could be easily implemented on clinical imaging systems, and yet have the potential to precisely extract fundamental MT parameters that provide information on the structure and behaviour of heterogeneous systems like biological tissues. The first step of the reformulation involves determining the "continuous wave power equivalent ($B_{1\mathrm{CWPE}}$)" of the MT pulses. We defined the CW power equivalent to be the root mean square (rms) value of the saturating field whose amplitude is given by:

$$\omega_{1\mathrm{CWPE}} = \gamma\sqrt{P_{\mathrm{SAT}}} = \gamma B_{1\mathrm{CWPE}} \quad (3)$$

where P_{SAT} is the mean square saturating field, averaged over a time TR'. For a 3DFT sequence, or a single-slice 2DFT sequence, TR' is equal to the sequence repetition time, TR; in the case of multislice 2DFT sequences, TR' is equal to the repetition time divided by the number of slices collected per TR, if, as is usually the case, one MT pulse is applied prior to each slice selective excitation pulse. We used the term "CW Power Equivalent" since the rates R_{RFA} and R_{RFB} (the rates of loss of longitudinal magnetisation in each of the pools due to the application of the MT pulse) are proportional to ω_1^2, i.e., the power of the MT pulse (as given by Eq. (2)).

An arbitrary shaped RF pulse, applied on resonance, results in an excitation flip angle θ (in degrees) which is a function of its shape (typically Gaussian or Sinc), whether it is windowed or not, (e.g., by Hanning or Hamming windows), its bandwidth (defined as fully width at half maximum), its duration (τ_{SAT}) and its maximum amplitude (B_{SAT}). Similarly, the effect of a shaped MT saturation pulse can be conveniently expressed by the effective flip angle, θ_{SAT} (in degrees), which would be given to the magnetisation if the pulse were applied on resonance. This can be written as:

$$\theta_{\mathrm{SAT}} = \left[\frac{180}{\pi}\right]\gamma p_1 B_{\mathrm{SAT}} \tau_{\mathrm{SAT}} \tag{4}$$

where γ is the gyromagnetic ratio of the proton and p_1 is the ratio of the mean amplitude of the saturation pulse to that of a rectangular pulse of the same amplitude. If θ_{SAT} is known (it is typically specified as an input to the scanner), B_{SAT} can thus be calculated. The mean square saturating field, averaged over the whole sequence (P_{SAT}), can then be determined from:

$$P_{\mathrm{SAT}} = p_2 B_{\mathrm{SAT}}^2 \frac{\tau_{\mathrm{SAT}}}{\mathrm{TR'}} \tag{5}$$

where p_2 is the ratio of the square of the mean amplitude of the saturation pulse to that of a rectangular pulse of the same height. Finally, substituting this in Eq. (3), the value of $\omega_{1\mathrm{CWPE}}$ can be determined.

2.3. The bound water lineshape

Since the protons in the semi-solid pool do not experience the motional narrowing experienced by the protons in the free pool [13], they cannot be characterised by the Lorentzian lineshape function that results from the Bloch formalism. It is common practice to represent the bound pool with a generalised lineshape function. Assuming a Gaussian lineshape to represent the rate of RF absorption by the semi-solid pool, R_{RFB} can be written (replacing ω^2 in Eq. (2) by ω^2_{CWPE}) as:

$$R_{\mathrm{RFB}} = \omega^2_{\mathrm{CWPE}} \sqrt{\frac{\pi}{2}}\, T_2^B \left(\exp \frac{(-2\pi\Delta f T_2^B)^2}{2} \right) \tag{6}$$

Alternatively, a super-Lorentzian lineshape can be used to represent the bound pool, and in this case, R_{RFB} can be written as:

$$\begin{aligned} R_{\mathrm{RRFB}} &= \omega^2_{\mathrm{CWPE}} \pi g(2\pi\Delta f) \\ &= \omega^2_{\mathrm{CWPE}} \pi \left[\int_0^{\pi/2} d\theta \, \sin\theta \sqrt{\frac{2}{\pi}} \frac{T_2}{(3\cos^2\theta - 1)} \right. \\ &\qquad \left. \times e^{-2[2\pi\Delta f T_2/3\cos^2\theta - 1]^2} \right] \end{aligned} \tag{7}$$

where θ is the angle between the external magnetic field and the axis of molecular orientation. Both lineshapes were investigated for the work reported here.

2.4. The signal equation for pulsed MT measurements and the bound water fraction "f"

Although Eq. (1) provides a useful expression describing the behaviour of magnetisation associated with the liquid pool under the influence of an MT pulse, it is dimensionally incorrect. In order to normalise their MT experiments, researchers have often equated M_0^A to 1 [13,14,16,17]. In order to maintain dimensionality on both sides of equation, however, it is necessary to keep M_0^A explicitly in the equation. The signal intensity obtained from the liquid pool, S, can then be written as:

$$S = gM_Z^A = gM_0^A \cdot \left(\frac{R_B\left[\frac{RM_0^B}{R_A}\right] + R_{\mathrm{RFB}} + R_B + RM_0^A}{\left[\frac{RM_0^B}{R_A}\right](R_B + R_{\mathrm{RFB}}) + \left(1 + \left[\frac{\omega_{\mathrm{CWPE}}}{2\pi\Delta f}\right]^2\left[\frac{1}{R_A T_2^A}\right]\right)(R_{\mathrm{RFB}} + R_B + RM_0^A)} \right) \tag{8}$$

where "g" is a scaling factor including the gain of the RF amplifier and other scanner dependant effects.

We now introduce a new parameter "f," which we define to be the bound water fraction, i.e.

$$f = \frac{M_0^B}{M_0^B + M_0^A} \tag{9}$$

We believe that 'f' is a more meaningful parameter to fit for, since it provides a much clearer insight into the biological significance of alterations in MT parameters in pathology, for example, in demyelination.

Rewriting Eq. (8) in terms of "f," we obtain:

$$S = gM_0^A \left(\frac{R_B\left[\frac{RM_0^A f}{R_A(1-f)}\right] + R_{\mathrm{RFB}} + R_B + RM_0^A}{\left[\frac{RM_0^A f}{R_A(1-f)}\right](R_B + R_{\mathrm{RFB}}) + \left(1 + \left[\frac{\omega_{\mathrm{CWPE}}}{2\pi\Delta f}\right]^2\left[\frac{1}{R_A T_2^A}\right]\right)(R_{\mathrm{RFB}} + R_B + RM_0^A)} \right) \tag{10}$$

While the model has eight fundamental parameters (T_1^A, T_2^A, T_1^B, T_2^B, M_0^A, f, R and g), the manner in which these are combined within the various terms of Eq. (10) means that only 6 values can be uniquely determined. This interdependence can be seen by considering, for example, the effect of a doubling of R and g, while halving M_0^A, which will give no change in the predicted MR signal. A similar interdependence exists for $R_A T_2^A$, and f. The 6 values that can be uniquely determined are therefore R_B, RM_0^A, $f/R_A(1-f)$, T_2^B (via R_{RFB}), $1/R_A T_2^A$ and gM_0^A.

2.5. Extraction of "f"—the bound water fraction

The parameter that we are often most interested in is the bound water fraction "f." In order to extract it explicitly on its own, knowledge of R_A, the relaxation rate of the free pool is required. The observed relaxation rate, $R_{A\mathrm{obs}}$, is related to R_A by the following expression [13]:

$$\begin{aligned} R_{A\mathrm{obs}} = \frac{1}{2}\Big[& RM_0^B + R_A + RM_0^A + R_B \\ & - \sqrt{(RM_0^B + R_A - RM_0^A - R_B)^2 + 4RM_0^A RM_0^B} \Big] \end{aligned} \tag{11}$$

This can be rearranged and written such that R_A is expressed

in terms of the fitted parameters, RM_0^A and $f/R_A(1-f)$ and the observed relaxation rate R_{Aobs}:

$$R_A = \frac{R_{Aobs}}{1 + \left(\frac{RM_0^A f}{(1-f)R_A} \frac{(R_B - R_{Aobs})}{(R_B - R_{Aobs}) + RM_0^A} \right)} \quad (12)$$

Knowing R_B, RM_0^A and $f/R_A(1-f)$ from the fitting routine, and the value of R_{Aobs} (by measuring it experimentally), R_A can be calculated. This value can then combined with the fitted value of $f/R_A(1-f)$ to yield f (the bound water fraction).

3. Experimental method

3.1. Data acquisition

The measurements were carried out on a whole-body 1.5 Tesla MRI system (GE Sigma, General Electric Medical Systems, WI, USA), using a standard birdcage transmit/receive head coil. The pulse sequence used was a locally implemented MT prepared Spoiled Gradient Echo (MTSPGR) sequence which consists of an MT pulse applied immediately before each excitation pulse of a standard 2DSPGR (Two Dimensional Spoiled Gradient Echo) sequence. The MT preparatory pulse chosen for this purpose was a Gaussian pulse of duration 14.6 ms applied at a specific offset frequency and amplitude. The flip angle of the spoiled gradient echo sequence was kept at an optimum value of 25° with an aim to minimise the degree of T1-weighting in the images whilst still producing images of diagnostic quality, i.e., images with clinically acceptable signal-to-noise ratio (SNR).

A matrix size of 256 × 96 was used, covering an FOV of 24 × 18 cm and giving nominal acquired pixel size of 0.94 × 1.88 cm. A partial k-space acquisition scheme, collecting only 24 lines of k-space on one side of $k = 0$ (i.e., 'NEX = 0.75'), was used to further reduce the number of phase encode steps, and thus scan time, required. With a TR of 1140 ms, this leads to a scan time of 82 s per measurement. All data were zero filled and padded during reconstruction, to give reconstructed images with a 256 × 256 matrix size over a 24 × 24 cm FOV. Table 1 shows the amplitudes calculated for the continuous wave power equivalent Gaussian MT pulse used in the *in-vitro* MT experiments.

3.2. In-vitro MT measurements

Quantitative MT measurements were made on human brain slices (7 normal and 4 MS), fixed in formalin. Five different MT powers were used for the quantitative *in-vitro* MT experiments; details are given in Table 1. For each amplitude of the MT pulse, 11 different offset frequencies were used (20, 50, 100, 300, 500, 800, 1000, 3000, 5000, 1000 Hz); thus 55 independent measurements were performed. Care was taken to ensure that the scanner transmitter and receiver gains remained constant throughout the acquisitions.

Table 1
Parameters, including continuous wave power equivalents, calculated for the Gaussian MT pulses used in the *in-vitro* MT experiments (p_1 = 0.4819, p_2 = 0.3441, τ_{SAT} = 14.6 ms)

Flip angle θ_{SAT} (°)	B_{SAT} (μT)	B_{1CWPE} (μT)	ω_{1CWPE} (rads^{-1})
285	2.64	0.93	707
420	3.90	1.37	1042
660	6.12	2.16	1638
940	8.72	3.06	2333
1460	13.55	4.75	3624

Fourteen slices were collected per acquisition, with TR/TE = 1140/12 ms. The scan time for each MT measurement (i.e., for each power/offset frequency combination) for 14 slices was 82.08 s, thus, the total scan time for the 55 combinations of MT power and offset frequency was ~75 minutes (for 14 contiguous slices).

3.3. In-vitro observed relaxation time (T_{1OBS}) measurement

The observed longitudinal relaxation time of the sample, T_{1OBS}, was measured using a simple, single-slice inversion recovery sequence (180° − inversion time − 90° − TE/2 − 180° − TE/2 − (spin echo)). Slice-selective 90° and 180° pulses were used; however, the slice profile of the 180° pulses were wider than the thickness of the excited slice to ensured that only the signal from the flat portion of their slice profile (where the tip angle is correct and relatively uniform) contributed to the acquired signal. The magnitude of the longitudinal magnetisation as a function of the inversion time was fitted to an exponential recovery function given by Eq. (13):

$$M_Z = M_0\left(1 - 2\alpha \exp\left[\frac{-\mathrm{TI}}{T_{1OBS}}\right] + \exp\left[\frac{-\mathrm{TR}}{T_{1OBS}}\right]\right) \quad (13)$$

where TI = inversion time, TR = repetition time, T_{1OBS} = longitudinal relaxation time, α = inversion efficiency term, M_0 = fully relaxed value of the magnetisation.

The repetition time (TR) was kept at 6000 ms (>5 T_{1OBS}) to allow the tissue to largely recover its magnetisation between subsequent RF pulses. Six inversion times (50, 400, 900, 1800, and 3000 ms) were used. Data was acquired using a 256 × 128 matrix, covering an FOV of 24 × 24 cm. Full k-space acquisition and a single signal average were used, giving a total measurement time of 76.8 minutes.

3.4. In-vitro data analysis

All images were transferred to a network of Sun workstations (Sun Microsystems Computer Corporation, Mountain View, CA) using GE supplied software (*xfer*). They were then converted to a variant of the UNC (University of North Carolina, Chapel Hill, NC) image format and displayed using the DispImage package [18]. Regions of interest representing areas of normal white matter (WM) and MS lesions were defined by a trained observer (CD) and the signal intensities for each of the ROIs of each image were determined. The value of $T_{1\text{obs}}$ for each region was determined from Eq. (13) using a simple non-liner least square algorithm. Quantitative MT parameters were obtained by fitting the binary spin bath model to the measured data, using a sum-of-square minimisation technique (downhill simplex method). Details of the Simplex method can be found in several texts [19,20,21].

Since quantitative MT experiments of this kind are largely insensitive to R_B, the relaxation rate of the bound pool, this parameter has been fixed arbitrarily to be 1 s^{-1} for all tissue types by several groups [10,13,16,17,22]. A similar approach was adopted in this study since the residual sum of squares was found to be insensitive to changes in R_B, i.e., in practice, this was found to have little impact on subsequent estimates of the other parameters. R_B tended to vary widely, and sometimes became negative (which is physically meaningless). R_B was therefore modified model to produce estimates of the five parameters, gM_0^A, RM_0^A, $f/R_A(1-f)$, $1/R_AT_2^A$, and T_2^B (via R_{RFB}), using a 6 vertex Simplex. We felt that this was justified since the correlation times associated with macromolecules such as globular proteins are thought to range from 10^{-5} to 10^{-8} s [23,24] and the corresponding T_1 relaxation time associated with the correlation time of $\sim 10^{-6}$ s are of the order of seconds. This modification has the added benefit of reducing the time required for fitting.

A Lorentzian lineshape was used to represent the rate of RF absorption by the liquid pool. Both Gaussian and Super-Lorentzian lineshapes were used for the semi-solid pool to describe the rate of loss of longitudinal magnetisation due to off-resonance irradiation; the Super-Lorentzian lineshape was found to fit the data better than the Gaussian lineshape (a reduction in the residual sum-of squares by 28%), in agreement with the work carried out by other groups for *in-vitro* bovine white matter [16] and *in-vivo* rat brain [17].

3.5. In-vivo MT experiments

Having ensured that the procedure was ready for use in humans, the process was then repeated on five normal healthy controls with no history of neurological or psychiatric problems and six patients with MS (three with relapsing-remitting MS and three with benign MS), all recruited from the National Hospital of Neurology and Neurosurgery. Local ethics approval was obtained from the Joint Ethics Committee of the National Hospital for Neurology and Neurosurgery and the Institute of Neurology, and all subjects gave informed written consent for the study. The patients underwent a neurological examination and evaluation of EDSS prior to undergoing MR imaging, and had a median Expanded Disability Status Scale (EDSS) of two.

In order to test for reproducibility of the MT parameters, one of the healthy controls was rescanned, after an interval of 10 months.

The same MTSPGR sequence that was used the *in-vitro* experiments was used for the *in-vivo* scans. However, since a scan time of ~75 minutes (for MT experiments) is clinically impractical, the number of MT measurements had to be reduced. The range of powers and offset frequencies used by the Henkelman group for their MT experiments on agar gels and bovine white matter [13,16], along with the experience gained by our own *in-vitro* experiments, were used to guide the choice of measurements to be retained. Due to specific absorption rate concerns, the maximum amplitude of the MT pulse that could be applied in our *in-vivo* experiments was 734 rads/s. Several combinations of MT power and offset frequency were used to re-fit subsets of Henkelman's ex vivo data, and the resulting parameters and their associated errors were extracted. The minimum number of measurements that could be used was found to be 10; any fewer resulted in large, unacceptable errors in the fitting procedure. The ten unique combinations of amplitude and offset frequency of the MT pulse chosen for the *in-vivo* MT measurements are given in Table 3.

In the *in-vivo* situation, 28 slices, of 5 mm thickness, were collected per acquisition, the repetition time between successive saturation pulses (TR') being 40 ms. Twenty-eight contiguous slices were acquired with an aim to achieve full brain coverage, i.e., from the apex of the head to the brain stem. All 28 slices were acquired in a single TR and the scan time for each measurement (i.e., acquisition time per power/offset frequency combination) for 28 slices was identical to the *in-vitro* case, i.e., 1 min + 22 sec. Thus, the total scan time for the 10 combinations of MT power and offset frequency was ~15 minutes.

3.6. In-vivo observed relaxation time (T_{1OBS}) measurement

Once again, an independent measurement of the observed relaxation time, $T_{1\text{OBS}}$ of the two-pool system was required to constrain the solution as before. In the *in-vivo* case this was carried out using the method of Parker et al. [30], which includes compensations for slice profile and B_1 inhomogeneity effects. The method requires acquisition of two gradient echo data sets at different repetition times, designed to create a predominantly PD weighted (PDW) and a heavily T_1 weighted (T_1W) data set, respectively. The acquisition parameters used were (TR/TE/flip angle/number of averages); 1500 ms/10 ms/90°/2 and 360 ms/10 ms/90°/8 for the PDW and T_1W acquisitions, respectively. Slice thickness and FOV were 5 mm and 24 cm respectively, to match the MT scans, and a matrix size of 256 × 256 was

used. The total measurement time is approximately 19 minutes, although this can be reduced, if necessary, at the expense of matrix size or signal averaging.

The total measurement time for the *in-vivo* MT experiments was 15 minutes (for the MT measurements plus 19 minutes (for the measurement of T_{1OBS}) = 34 minutes.

3.7. In-vivo data analysis

All images were again transferred to a network of Sun, converted to a variant of the UNC image format and displayed using the DispImage package. T_1 maps were calculated on a pixel by pixel basis, using the method Parker et al. [30]. Regions of interest were then defined, and the signal intensities for each ROI was determined for each of the acquired MT weighted images, plus the calculated T_1 image. While choosing an ROI from a particular slice, the slice above and below the one chosen were also inspected, to reduce the likelihood of any contamination between WM and GM in each single image due to through slice partial volume effects. ROIs were defined to cover three specific areas of white matter (occipital white matter, frontal white matter, and centrum semiovale) and two specific areas of grey matter (cortical grey matter, and cerebral grey matter). Data was collected from both the left and right hemispheres for each of these regions. Thus, a total of 10 ROIs were collected in healthy controls. In the patient group, the same 10 regions were investigated, with the addition of a variable number of additional ROIs representing lesions. In order to assess inter-rater covariance, ROIs were independently outlined on one representative patient dataset by two different trained observers (CD and GD); data was collected from 17 ROIs in each case.

As with the *in-vitro* MT experiments, the quantitative *in-vivo* MT data was fitted to the equation for signal intensity of the free pool, i.e., Eq. (10). However, unlike the *in-vitro* case, the Gaussian lineshape seemed to provide a better fit between experiment and theory (an improvement of ~30% in the residual sum of squares as compared to the super-Lorentzian lineshape). Quantitative MT measurements along with the fit of the signal equation for two lineshapes (Gaussian (A) and super-Lorentzian (B) are shown in Fig. 1

For (qualitative) comparison purposes, MT ratios, expressed in percent units (p.u.), were also calculated for different regions-of-interest (ROI) using the expression:

$$\mathrm{MTR} = 100 * \left[\frac{S_{\mathrm{SAT}} - S_{\mathrm{UNSAT}}}{S_{\mathrm{SAT}}} \right] \tag{14}$$

where S_{SAT} and S_{UNSAT} are the mean saturated and unsaturated signal intensities in the ROI respectively. A combination of flip angle/offset frequency = 843°/1000 Hz was used to obtain the saturated signal intensity and a combination of 434°/15000 Hz was used to obtain the 'unsaturated' (or more correctly 'less saturated') signal intensity. Fig. 2 shows (A) grey matter data and (B) MS lesion data fitted to Eq. (10) using a Gaussian lineshape.

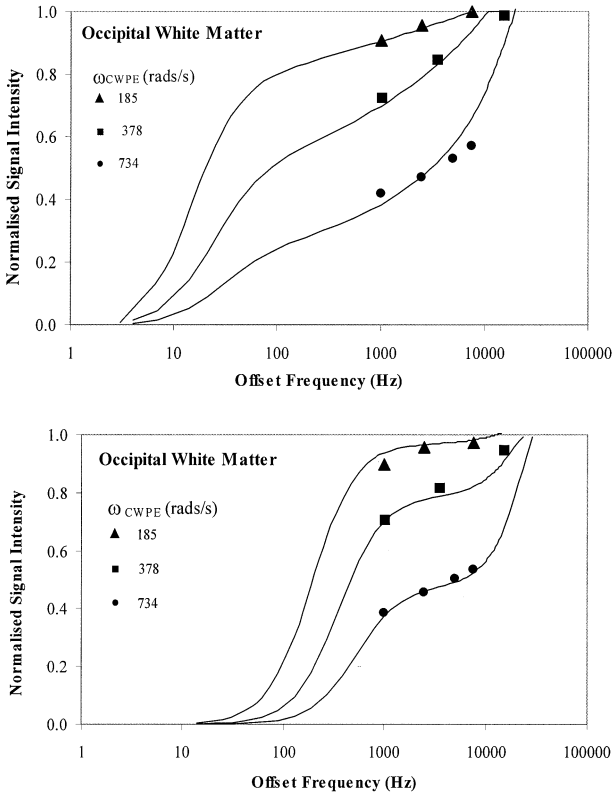

Fig. 1. Typical graphs showing the fitting of the model to *in-vivo* measurements of normal occipital white matter. Graph (A) shows the model fitted with a super-Lorentzian to describe the rate of RF absorption of the semi-solid pool and (B) shows the same data but using a lineshape Gaussian lineshape instead. The Gaussian lineshape gives a better fit to the data (a reduction in the residual sum-of-squares by 30%). In both graphs the solid lines are a fit of Eq. (10) to the data, the three lines representing the three powers used in the experiment.

4. Results

4.1. In-vitro results

Parameter estimates obtained for 7 normal white matter and 5 MS lesions from fixed human brain slices are shown in the Table 2.

The results obtained can be summarised as follows:

1. *In-vitro* MT parameters were successfully estimated from the MT effect at 55 combinations of power and offset frequencies.
2. In comparison to normal white matter, the MS lesions demonstrated an increase in the transverse relaxation time of the bound pool (T_2^B).
3. More important, a dramatic reduction was found in f (the bound water fraction) in the MS lesions, which is consistent with demyelination.

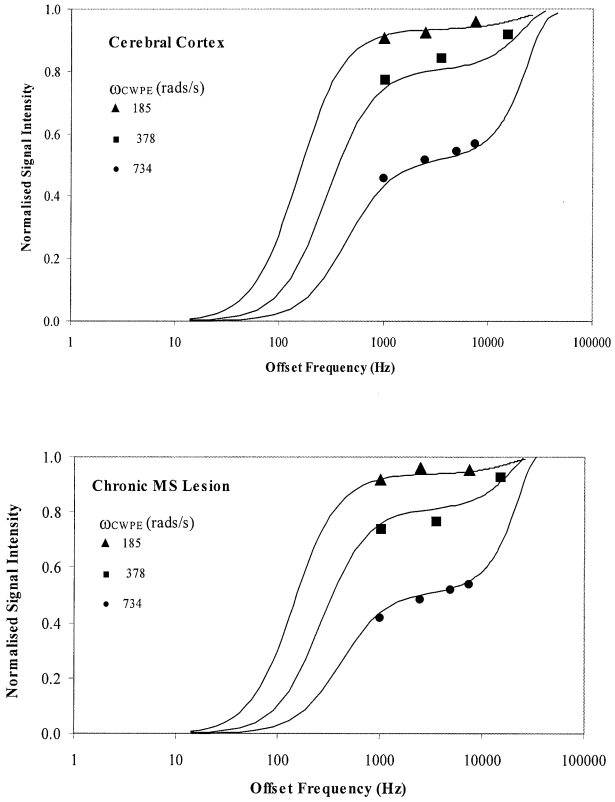

Fig. 2. Magnetisation transfer *in-vivo* data for (A) cerebral cortex and (B) MS lesion.

4. $1/R_A T_2^A$, the ratio of the longitudinal relaxation time to the transverse relaxation time of the free pool, was found to be slightly higher in the MS samples.
5. The observed relaxation time (T_{1OBS}) was found to be higher in MS lesions compared to normal white matter.
6. The observed longitudinal relaxation times (T_{1OBS}) for both normal WM and MS WM are considerably lower than the values found in the literature (for *in-vivo* brain [25,26]). We attribute this difference to the effect of formalin fixation; several researchers [27,28,29] have measured the relaxation times of formalin-fixed tissues and found a significant reduction in relaxation times.

Table 2
Fitted parameters for *in-vitro* brain samples (normal and MS)

Parameter	Normal WM (n = 7)	MS tissue (n = 5)
RM_A^0 (s^{-1})	1831 ± 291	3213 ± 300
$f/R_A(1-f)$ (s^{-1})	0.07 ± 0.07	0.006 ± 0.004
T_2^B (μs)	13.1 ± 6.8	20.2 ± 1.9
$1/R_A T_2^A$	1.6 ± 0.3	1.8 ± 0.7
gM_0^A	363 ± 27	426 ± 14
T_{1obs} (s)	0.38 ± 0.02	0.47 ± 0.01
T_1^A (s)	0.37 ± 0.08	0.49 ± 0.01
T_2^A (s)	0.24 ± 0.04	0.31 ± 0.18
f	0.14 ± 0.11	0.02 ± 0.009

Table 3
The ten unique combinations of amplitude and offset frequency of the MT pulse used *in-vivo*

Flip angle θ_{SAT} (in °)	Amplitude of the CWPE MT pulse ω_{1CWPE} (in radians/s)	Offset frequency (in Hz)
212	185	1000
212	185	2500
212	185	7500
434	378	1000
434	378	3500
434	378	15000
843	734	1000
843	734	2500
843	734	5000
843	734	7500

4.2. In-vivo results

In-vivo MT parameter estimates obtained from healthy controls (Table 4), normal appearing white matter in patients with MS (Table 5) and MS lesions (Table 6) have been summarised. The results obtained can be summarised as follows:

1. *In-vivo* MT parameters were successfully estimated from MT effect at 10 combinations of power and offset frequencies.
2. In comparison to normal white matter, the MS lesions demonstrated a statistical decrease ($p < 0.001$) in the transverse relaxation time of the bound pool (T_2^B).
3. More important, a dramatic reduction was found in f (the bound water fraction) in the MS lesions ($p < 0.001$), despite some regions having normal MTR values.
4. The observed relaxation time (T_{1OBS}) was found to be higher in MS lesions compared to normal white matter.
5. Reproducibility of the MT parameters, assessed as the scan-rescan coefficient of variation over all WM ROIs, was found to be 2% and 3% respectively for f and T_2^B.
6. The inter-rater coefficients of variation in f and T_2^B (again over all WM ROIs) were found to be 7% and 4.5% respectively.

5. Discussion

5.1. Bound water pool lineshape

In our *in-vitro* studies we found that, in agreement with other workers, the use of a super-Lorentzian lineshape for

Table 4
In-vivo MT parameters for healthy controls (n = 5)

	Occipital white matter	Frontal white matter	Centrum semiovale	Cortex	Cerebellum
RM_0^A (s^{-1})	3070 ± 1986	2258 ± 1239	2239 ± 1193	3075 ± 1068	3544 ± 1226
$f/R_A(1-f)$ (s^{-1})	0.11 ± 0.01	0.11 ± 0.01	0.11 ± 0.01	0.10 ± 0.01	0.10 ± 0.01
T_{2B} (μs)	17.8 ± 1.4	18.3 ± 0.9	18.5 ± 1.0	16.6 ± 2.8	16.3 ± 0.6
$1/R_AT_2^A$	44 ± 6	45 ± 5	44 ± 6	27 ± 7	32 ± 3
gM_0^A	366 ± 34	366 ± 32	364 ± 31	449 ± 40	419 ± 34
T_{1obs} (s)	0.62 ± 0.04	0.61 ± 0.04	0.61 ± 0.02	1.19 ± 0.10	1.10 ± 0.11
T_1^A (s)	0.58 ± 0.05	0.57 ± 0.05	0.57 ± 0.03	1.21 ± 0.11	1.11 ± 0.12
T_{2A} (s)	0.01 ± 0.01	0.01 ± 0.01	0.01 ± 0.01	0.05 ± 0.01	0.03 ± 0.01
f	0.16 ± 0.01	0.16 ± 0.01	0.16 ± 0.02	0.08 ± 0.01	0.09 ± 0.01
MTR (p.u.)	59.2 ± 0.9	59.9 ± 0.7	60.1 ± 0.8	52.3 ± 3	55.6 ± 1.1

the bound water pool gave the best results (as evidenced by a reduction in the residual sum of squares (30%) relative to a fitting with a simple Gaussian lineshape). *In-vivo*, however, we obtained better fits for the Gaussian function. This is in conflict with the work carried out on bovine tissue [16], *in-vivo* rat brain [17], and human *in-vivo* brain [7,10,12] where a super-Lorentzian lineshape has been used to describe the bound pool. The super-Lorentzian described in articles from the Henkelman group did not fit our *in-vivo* data perfectly and it is likely that the Gaussian lineshape provides a better fit over the small range of data points presented here. This would also apply when comparing this work to that of Sled and Pike [10] as a large number of data points were collected for that work. This could mean that further improvements can be made if more careful selection of the data points is made; however it is unclear at this time if this would lead to significant differences in the parameters.

In fact, various a priori lineshapes have been used to describe the absorption lineshape of the semi-solid pool. A three-pool model to conduct MT experiments in agar gels [31] consisted of water and mobile polymers having a Lorentzian lineshape while the macromolecules of the bound pool were characterised by a Gaussian lineshape. The same lineshape has also been used in a three-pool MT model to fit data in cartilage [32] and in a two-pool model for bovine serum albumin [33]. Recently, a Gaussian lineshape has been used to represent the bound pool in a three-pool MT model for hydrated cross-linked bovine serum albumin [34]. Two other lineshapes (a "flexible" lineshape based an average numerical lineshape extracted from experimental MT data and a "Kubo-Tomita" lineshape [35]) have also been used to extract MT parameters from bovine tissues as published in ref. [16]. More work is necessary to determine whether our result is of biological significance, or simply reflects the inability of the fitting procedure to extract accurate parameters from the more complex super-Lorentzian lineshape given our low number of input measurements.

5.2. *Fitted* RM_0^A *values*

The parameter appears to vary very little between different regions in the brain. A possible explanation for this is the likelihood that the two pools are extremely well coupled; clearly this parameter does not seem to have diagnostic potential (unlike parameters f and T_2^B).

Table 5
In-vivo MT parameters for normal appearing white matter in patients with MS

	Occipital white matter (n = 6)	Frontal white matter (n = 7)	Centrum semiovale (n = 6)	Cortex (n = 6)	Cerebellum (n = 7)
RM_0^A (s^{-1})	3371 ± 1578	3644 ± 1891	2958 ± 939	3983 ± 879	2857 ± 1267
$f/R_A(1-f)$ (s^{-1})	0.11 ± 0.01	0.10 ± 0.01	0.10 ± 0.01	0.10 ± 0.02	0.10 ± 0.01
T_{2B} (μs)	17.9 ± 1.1	18.7 ± 0.9	18.8 ± 0.7	14.6 ± 1.6	17.2 ± 1.5
$1/R_AT_2^A$	42 ± 6	42 ± 5	40 ± 6	15 ± 11	30 ± 7
gM_0^A	389 ± 62	374 ± 52	353 ± 80	473 ± 33	409 ± 43
T_{1obs} (s)	0.73 ± 0.10	0.66 ± 0.07	0.68 ± 0.07	1.32 ± 0.26	1.08 ± 0.17
T_1^A (s)	0.70 ± 0.11	0.63 ± 0.08	0.64 ± 0.07	1.35 ± 0.29	1.09 ± 0.19
T_{2A} (s)	0.02 ± 0.01	0.02 ± 0.01	0.02 ± 0.01	0.08 ± 0.13	0.04 ± 0.01
f	0.13 ± 0.02	0.14 ± 0.02	0.14 ± 0.02	0.07 ± 0.03	0.08 ± 0.01
MTR (p.u.)	58.9 ± 1	59.5 ± 1	59.3 ± 1	48.8 ± 6	55.5 ± 1

Table 6
In-vivo MT parameters in MS lesions

	Left occipital lesion (n = 5)	Right occipital lesion (n = 3)	Left periventricular lesion (n = 3)	Left centrum semiovale lesion (n = 3)	Right centrum semiovale lesion (n = 4)
RM_0^A (s^{-1})	3590 ± 2285	4295 ± 710	3322 ± 911	2257 ± 1499	2128 ± 1533
$f/R_A(1-f)$ (s^{-1})	0.11 ± 0.01	0.11 ± 0.02	0.11 ± 0.01	0.10 ± 0.01	0.11 ± 0.01
T_{2B} (μs)	16.3 ± 0.9	16.1 ± 0.5	16.1 ± 1.4	16.2 ± 0.9	16.6 ± 1.2
$1/R_AT_2^A$	29 ± 12	28 ± 11	30 ± 11	27 ± 3	25 ± 5
gM_0^A	457 ± 84	502 ± 40	445 ± 25	497 ± 70	468 ± 73
T_{1obs} (s)	1.05 ± 0.21	1.18 ± 0.16	1.26 ± 0.04	1.06 ± 0.38	0.99 ± 0.13
T_1^A (s)	1.05 ± 0.23	1.20 ± 0.17	1.29 ± 0.04	1.07 ± 0.42	0.99 ± 0.14
T_{2A} (s)	0.04 ± 0.01	0.05 ± 0.03	0.05 ± 0.02	0.04 ± 0.01	0.04 ± 0.01
f	0.09 ± 0.02	0.09 ± 0.02	0.08 ± 0.01	0.10 ± 0.04	0.10 ± 0.01
MTR (p.u.)	55.3 ± 2	55.2 ± 3	54.9 ± 4	55.1 ± 1	55.2 ± 1

5.3. Fitted T_2^B values

Short T_2^B relaxation values (between 14 μs and 19 μs) were found for all tissues investigated in this study (both in-vitro and *in-vivo*), and are consistent with the fitted values obtained by other workers. Others have measure a T_2^B of 8 μs for integral membrane protein rhodopsin [36] and a value of 9 μs for denatured egg white [37]. A simple two pool MT model [16] for bovine WM yielded 18 μs while a four-pool for the same type of tissue [38] yielded a value of 17 μs. Recently a value of 11 μs for *in-vivo* human WM [10] has been obtained.

Statistically significant differences were found between normal WM (in controls) and MS lesions ($p < 0.001$), indicating the possibility of this parameter to reflect changes in pathology.

5.4. Fitted $1/R_AT_2^A$ values and direct saturation effects

The ratio of measured T_{1obs}/T_{2obs} ratios can be used to estimate direct saturation effects. However, measured relaxation times give a weighted average of the relaxation contributions from all tissue components and also suffer from the effect of the presence of macromolecules on the observed relaxation times. The parameter $1/R_AT_2^A$, one of the outputs of the fitting procedure, can also be used to evaluate direct saturation effects on the water pool by the MT pulse. Differences between fitted and measured relaxation ratios have been reported by other workers [22,39] suggesting that the fitted values give the best estimate of direct saturation effects. In the present study, the parameter $1/R_AT_2^A$ shows statistically significant differences ($p < 0.001$) between NAWM and MS lesions and also between grey matter in patients and controls, thus indicating the possibility of subtle changes in grey matter, apart from the more obvious changes in white matter as a result of pathology.

The amount of direct saturation experienced by the water protons depends on the pulse strength ω_1, the offset frequency Δf and the values of (obtained from the fitting procedure).

$$\left[\frac{M_Z^A}{M_0^A}\right]_{DS} = \frac{1}{\left[1+\left(\frac{\omega_{CWPE}}{2\pi\Delta f}\right)^2\left(\frac{1}{R_AT_2^A}\right)\right]} \quad (15)$$

Fig. 3 shows the direction saturation effects calculated for the *in-vivo* data for two different pulse powers and a range of offset frequencies. The effects are similar for occipital white matter, frontal white matter and centrum semiovale in healthy controls. Regions with grey matter (cerebral cortex and cerebellum) with their lower $1/R_AT_2^A$ values are affected to a lesser extent than regions with white matter. Differences in direct saturation values between control and MS patients can also be seen in Fig. 3, these effects being greatest at offset frequencies below 1 kHz. Conventional MT ratios are unable to reflect these direct saturation effects, and the differences in MTR values between healthy controls and MS patients (and also between white and grey matter in controls) are likely to have at least some contribution from the effects of direct saturation.

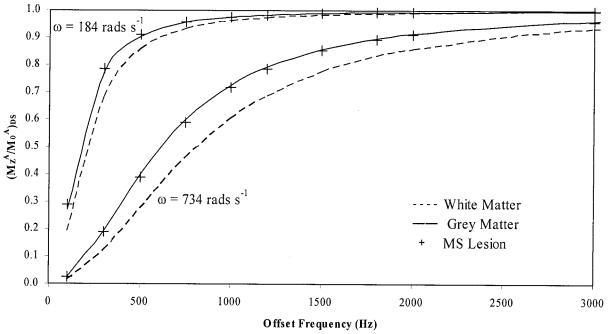

Fig. 3. Direct saturation effects for white matter, grey matter and MS lesions.

5.5. Clinical interpretation

While a detailed discussion of the clinical implications is beyond the scope of this paper, our preliminary results include a number of interesting features, in particular the reduction in f (the bound water fraction) in the MS lesions, which is seen even in some regions having normal MTR values. Two other parameters $1/R_A T_2^A$ and T_2^B also appear to be altered in MS lesions; in addition f is also altered in NAWM. Clearly, these parameters contain additional information that cannot gleaned from conventional MTR values. It is possible that gliosis may have replaced the myelin with glial cells (which still have a high bound water content) in such regions, leading to a maintained MTR. The decreased f, then, may be a function of disease progression, as demyelination sets in. Such hypotheses can only be confirmed (or rejected), however, by scanning many more patients with a variety of lesions of different ages. Such scanning is now underway.

Since an important therapeutic goal in MS is to promote remyelination, it is essential to monitor this repair process *in-vivo*. We believe that the MT parameters, particularly, f and T_2^B, are potentially capable of detecting and monitoring not just demyelination, but also remyelination *in-vivo*. This methodology can prove useful in determining the degree of spontaneous and therapeutically induced tissue reorganisation and remyelination in MS lesions, and thus validating therapeutic treatments for myelin repair.

6. Conclusion

The MT methods described above allow quantitative *in-vivo* imaging of all the observable MT parameters of the binary spin bath model. Specifically, the model yields the fractional size of the bound pool, the magnetisation exchange rate, the transverse relaxation time of the bound pool as well as the relaxation times of the free pool. For the first time, these parameters have been obtained from the whole brain in clinically feasible times. Unlike conventional MT ratios, these parameters are (relatively) independent of the details of the pulse sequences used to measure them, and have the potential to give new information about tissue composition and structure.

The two-pool model is, of course, only an approximation to the true, *in-vivo*, situation, and mathematical models with three [31,32,34] and four [38,40] pools have also been used to describe the MT phenomena occurring in tissue. Although these models might be more accurate than the two-model, the mathematical formulae describing the signal evolution are far more complex and the parameters extracted are more difficult to interpret. The models also requires a greater number of parameters to be experimentally measured (to extract some of the intrinsic MT parameters), resulting in impractical scan times. Clearly, there is a trade-off between the accurate description of the MT processes occurring in heterogeneous systems like biological tissue and practicality with which they can be implemented on clinical scanners. Researchers are continuously trying to create realistic and yet simple MT models that mimic the behaviour of biological tissues.

Heterogeneous systems like white matter have been described as complex matrices of macromolecules with water filling some of the spaces in these matrices and thus forming water compartments with different levels of mobility [40]. The dynamics involved in the contribution of the different water compartments to the observed effects of the free water pool have not yet been well characterised. Exchange of water between the various compartments alters the population of the water molecules and hence, on the time scale of this exchange, the observed properties of the free pool are a weighted average of the properties of the different water compartments. Our two-pool model is likely to be a simplified version of a multi-compartmental consisting of several water compartments and their associated exchange pathways. However, it has the advantage of being simple and easy to implement on clinical scanners, and provides parameters of the human brain within a relatively short period [41].

Acknowledgments

The NMR Research Unit is funded by the Multiple Sclerosis Society of Great Britain and Northern Ireland. The authors thank Drs. Gerard Davies and Claudia Wheeler-Kingshott and Mr. David MacManus and for assisting with the collection of *in-vivo* MT data.

References

[1] Pike GB, De Stefano N, Narayanan S, Worsley KJ, Pelletier D, Francis GS, Antel JP, Arnold DL. Multiple sclerosis: magnetization transfer MR imaging of white matter before lesion appearance on T2-weighted images. Radiology 2000;215(3):824–30.

[2] Lycklama A, Nijeholt GJ, Castelijns JA, Lazeron RH, van Waesberghe JH, Polman CH, Uitdehaag BM, Barkhof F. Magnetization transfer ratio of the spinal cord in multiple sclerosis: relationship to atrophy and neurologic disability. J Neuroimaging 2000;10(2):67–72.

[3] Rovaris M, Horsfield MA, Filippi M. Correlations between magnetization transfer metrics and other magnetic resonance abnormalities in multiple sclerosis. Neurology 1999;53(5 Suppl 3):S40–5. Review.

[4] Berry I, Barker GJ, Barkhof F, Campi A, Dousset V, Franconi J, Gass A, Schreiber W, Miller DH, Tofts PS. A multicenter measurement of magnetization transfer ratio in normal white matter. J Magn Reson Imaging 1999;9:441–6.

[5] Eng J, Ceckler TL, Balaban RS. Quantitative 1H magnetization transfer *in-vivo*. J Magn Reson 1991;17:304.

[6] McGowan JC, Schnall MD, Leigh JS. Magnetization transfer imaging with pulsed off-resonance saturation: variation in contrast with saturation duty cycle. J Magn Reson Imaging 1994;4:79–82.

[7] Chai JW, Chen C, Chen JH, Lee SK, Yeung HN. Estimation of in vivo proton intrinsic and cross-relaxation rate in human brain. Magn Reson Med 1996;36(1):147–52.

[8] Gochberg DF, Kennan RP, Robson MD, Gore JC. Quantitative imaging of magnetization transfer using multiple selective pulses. Magn Reson Med 1999;41:1065–72.
[9] Lee RR, Dagher AP. Low power method for estimating the magnetization transfer bound-pool macromolecular fraction. J Magn Reson Imag 1997;7:913–7.
[10] Sled JG, Pike GB. Quantitative imaging of magnetization transfer exchange and relaxation properties *in vivo* using MRI. Magn Reson Med 2001;46:923–31.
[11] Goldman M. Spin temperature and nuclear magnetic resonance in solids. London: Oxford University Press, 1970.
[12] Yarnykh VL. Pulsed Z-spectroscopic imaging of cross-relaxation parameters in tissues for human MRI: theory and clinical applications. Magn Reson Med 2002;47:929–39.
[13] Henkelman RM, Huang X, Xiang Q, Stanisz GJ, Swanson SD, Bronskill MJ. Quantitative interpretation of magnetization transfer. Magn Reson Med 1993;29:759–66.
[14] Graham SJ, Henkelman RM. Evaluating pulsed magnetization transfer imaging technique. Radiology 1999;212:903–10.
[15] Ramani A, Tofts PS. Comparison of continuous wave theory to pulsed multicentre MT data. In: Book of abstracts: Ninth annual meeting of the society of magnetic resonance in medicine, Vol. 2. Denver: ISMRM, 2000. p. 2078.
[16] Morrison C, Henkelman RM. A model for magnetisation transfer in tissues. Magn Reson Med 1995;33(4):475–82.
[17] Quesson B, Thiaudiere E, Delalande C, Dousset V, Chateil JF, Canioni P. Magnetization transfer imaging *in vivo* of the rat brain at 4.7 T: interpretation using a binary spin-bath model with a superLorentzian lineshape. Magn Reson Med 1997;38(6):974–80.
[18] Plummer DL. Dispimage: a display and analysis tool for medical images. Rivista di Neuroradiologia (Italy) 1992;5:489–95.
[19] Box MJ, Davies D, Swann WH. Non-linear optimisation techniques (monograph no. 5). Edinburgh: Oliver and Boyd, 1969.
[20] Bunday BD. Basic optimisation methods. Edward Arnold Ltd, 1984.
[21] Press WH, Teukolsky SA, Vetterling WT, Flannery BP. Numerical recipes in C. New York: Cambridge University Press, 1992.
[22] Manson JC. Development and application of magnetisation transfer techniques and the study of proton magnetic resonance relaxation in acute leukaemia. Ph.D. Thesis, Department of Bio-Medical Physics and Bio-Engineering, University of Aberdeen, UK.
[23] Koenig SH, Brown RD III, Ugolini R. Magnetization transfer in cross-linked bovine serum albumin solutions at 200 MHz: a model for tissue. Magn Reson Med 1993;29(3):311–6.
[24] Fullerton GD. Biomedical magnetic resonance imaging. Werli FW, Shaw D, Kneeland JB. St. Louis: VCH Publisher, 1988.
[25] Kingsley S, Ogg RJ, Reddick W. Correction of errors caused by imperfect inversion pulses in MR imaging measurement of T1 relaxation times. Magn Reson Imaging 1998;16:1049–55.
[26] Stevenson VL, Parker GJM, Barker GJ, Birnie K. Variation in T1 and T2 relaxation times of normal appearing white matter and lesions in multiple sclerosis. J Neurol Sci 2000;178:81–7.
[27] Thickman DI, Kundel HL, Wolf G. Nuclear magnetic resonance characteristics of fresh and fixed tissue: the effect of elapsed time. Radiology 1983;148:183–5.
[28] Nagara H, Inoue T, Kitaguchi T, Tateishi J, Goto I. Formalin fixed brains are useful for magnetic resonance imaging study. J Neuro Sci 1987;81:67–77.
[29] Tovi M, Ericsson A. Measurements of T1 and T2 over time in formalin-fixed human whole-brain specimens. Acta Radiol 1992; 33(5):400–4.
[30] Parker GJ, Barker GJ, Tofts PS. Accurate multislice gradient echo T(1) measurement in the presence of non-ideal RF pulse shape and RF field nonuniformity. Magn Reson Med 2001;45(5):838–45.
[31] Tessier JJ, Dillon N, Carpenter TA, Hall LD. Interpretation of magnetisation transfer and proton cross-relaxation spectra of biological tissues. J Magn Reson 1995;107(Series B):138–44.
[32] Adler RS, Swanson SD, Yeung HN. A three-component model for magnetization transfer. Solution by projection-operator technique, and application to cartilage. J Magn Reson B 1996;110(1):1–8.
[33] Iino M. Transition from Lorentzian to Gaussian line shape of magnetization transfer spectrum in bovine serum albumin solutions. Magn Reson Med 1994;32(4):459–63.
[34] Ceckler T, Maneval J, Melkowits B. Modeling magnetization transfer using a three-pool model and physically meaningful constraints on the fitting parameters. J Magn Reson 2001;151(1):9–27.
[35] Li JG, Graham SJ, Henkelman RM. A flexible MT lineshape derived from tissue experimental data. Magn Reson Med 1997;37:866–71.
[36] Bloom M, Holmes KT, Mountford CE, Williams PG. Complete proton magnetic resonance in whole cells. J Magn Reson 1986;69: 73–91.
[37] Swanson SD. Transient and steady-state effects of indirect RF saturation in heterogeneous systems. In: Book of abstracts: Eleventh annual meeting of the society of magnetic resonance in medicine, Vol. 2. Berlin: SMRM; 1992. p. 255.
[38] Stanisz GJ, Kecojevic A, Bronskill MJ, Henkelman RM. Characterizing white matter with magnetization transfer and T2. Magn Reson Med 1999;42:1128–36.
[39] Hurst GH, Duerk J. A method for discrete numerical estimation of semi-solid lineshape from MT “Z Spectra” and initial application to phantom, *in vitro* and human *in vivo* samples. In: Book of abstracts: Third annual meeting of the society of magnetic resonance in medicine, Vol. 2. Nice: SMRM, 1995. p. 1035.
[40] Harrison R, Bronskill MJ, Henkelman RM. Magnetisation transfer and T2 relaxation components in tissue. Magn Reson Med 1995;33: 490–6.